Available online at www.sciencedirect.com
SCIENCE DIRECT®
Physics Letters A 318 (2003) 71–77
PHYSICS LETTERS A
www.elsevier.com/locate/pla

Amplitude modulation in a pair of time-delay coupled external-cavity semiconductor lasers

Awadhesh Prasad [a], Ying-Cheng Lai [a,b,*], Athanasios Gavrielides [c], Vassilios Kovanis [c]

[a] *Department of Mathematics and SSERC, Arizona State University, Tempe, AZ 85287, USA*
[b] *Departments of Electrical Engineering and Physics, Arizona State University, Tempe, AZ 85287, USA*
[c] *Nonlinear Optics Center, Air Force Research Laboratory, DELO, Kirtland AFB, NM 87117, USA*

Received 11 May 2002; received in revised form 4 October 2002; accepted 6 August 2003

Communicated by A.R. Bishop

Abstract

The phenomenon of amplitude death in coupled nonlinear oscillators has been a topic of recent interest. We demonstrate that a similar phenomenon can occur in a pair of time-delay coupled, external-cavity semiconductor lasers. In particular, with coupling chaotic oscillations of the laser field can be converted into quasiperiodic motion and low-frequency fluctuations in laser power can be suppressed.

PACS: 42.65.Sf; 42.55.Px; 05.45.-a

There has been an interest in the phenomenon of *amplitude death* [1–3] in the context of time-delay coupled limit-cycle oscillators [4,5]. The phenomenon was first observed in coupled chemical oscillators [1]. It was then established theoretically that, if the coupling is sufficiently strong and the spread in the natural frequencies of the oscillators is sufficiently broad, the amplitudes of the oscillations can reach zero [2,3]. The issue of time-delayed coupling, which is physically important, was recently addressed both theoretically [4] and experimentally [5]. An interesting result is that in the presence of a time delay, amplitude death can occur even if the natural frequencies of the limit-cycle oscillators are all identical [4], in sharp contrast to the situation of zero time delay, where a broad distribution in the natural frequencies of the oscillators is necessary for the amplitude death [2,3]. Since time delay is present in many physical applications, amplitude death may be pervasive in coupled oscillators. The aim of this Letter is to present evidence that a similar phenomenon can occur in time-delay coupled, external-cavity semiconductor lasers. The observable phenomenon is that the laser oscillation can be modulated significantly. We call the phenomenon *amplitude modulation* in coupled semiconductor lasers.

In many applications of semiconductor lasers, optical feedbacks are deliberately introduced to improve the performances of the laser such as the enhancement of the single longitudinal mode operation, spectral line narrowing, improved frequency stability, and

* Corresponding author.
E-mail address: yclai@chaos1.la.asu.edu (Y.-C. Lai).

0375-9601/$ – see front matter
doi:10.1016/j.physleta.2003.08.072

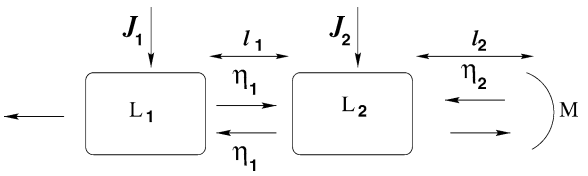

Fig. 1. Our coupling scheme generating amplitude modulation in external-cavity semiconductor lasers.

wavelength tunability, etc. [6]. However, at moderate feedback levels, which can be anticipated in most applications, the laser power can exhibit sudden, down-to-zero dropouts at random times, followed by a slow and gradual recovery after each dropout. The phenomenon is most serious when the pumping current is close to the solitary threshold. The average frequency of the dropouts is typically at the MHz-level, which is several orders of magnitude smaller than that of the solitary laser relaxation oscillation, hence the term low-frequency fluctuations (LFFs). In most applications, LFFs are undesirable. As we will show, our amplitude-modulation phenomenon can be used to potentially suppress the LFFs.

We consider a pair of coupled semiconductor lasers, as schematically illustrated in Fig. 1. Two laser diodes, denoted by L_1 and L_2, are mutually coupled through a coupling parameter $\eta_1 < 1$, i.e., a η_1 fraction of the laser field of L_1 is injected into L_2 and vice versa. Laser L_2 is subject to an additional optical feedback, characterized by the external mirror M with reflection coefficient η_2. The physical distance between L_1 and L_2 is l_1 and the length of the external cavity of L_2 is l_2. We shall demonstrate that with the coupling scheme, which can be implemented in laboratory experiments, the optical output from the laser L_1 can be modulated so that its maximum values are decreased but its minimum values, which is zero when it is uncoupled with L_2 and subject to optical feedbacks from M, is bounded away from zero. The average power of the output from L_1 maintains at approximately the same level as that in the absence of coupling. Such sustained operation of the laser without complete power dropouts occurs in parameter regions of positive measure.

The fundamental equations modeling a single external-cavity semiconductor laser is a set of delay-differential equations, known as the Lang–Kobayashi (LK) equations [7], which describe the time evolutions of the complex electrical field $E(t)$ of a single longitudinal mode and the carrier density $n(t)$ averaged spatially over the laser medium. The equations can be written in a standard normalized form [8]

$$\frac{dE(t)}{dt} = (1+i\alpha)N(t)E(t) + \eta e^{-i\omega_0\tau}E(t-\tau),$$
$$T\frac{dN(t)}{dt} = J - N(t) - [2N(t)+1]|E(t)|^2, \qquad (1)$$

where α is the linewidth enhancement factor [9], ω_0 is the angular frequency of the solitary laser, τ_p is the photon life time, τ_s is the carrier lifetime, $J \equiv \mathcal{J} - \mathcal{J}_{\rm th}$ ($\mathcal{J}$ is the injected constant current density and $\mathcal{J}_{\rm th}$ is the threshold), $N(t) \equiv n(t) - n_{\rm th}$, and $n_{\rm th} = \tau_p^{-1}$ is the threshold carrier density for the solitary laser. The external cavity is characterized by two parameters: (i) the coefficient γ characterizing the relative amount of light reflected back into the laser cavity, and (ii) the delay time $\tau = 2L/c$ that is the round-trip time of the light in the external cavity of length L. The gain per unit time of the single longitudinal mode is $G(n, E) = G_n[n(t) - n_0](1 - \epsilon|E(t)|^2)$, where G_n is the modal gain coefficient, n_0 is the carrier density at transparency, and ϵ is the gain saturation coefficient. In regimes of LFFs, typically $\epsilon \approx 0$ so that, approximately, $G(n, E)$ does not depend on the electrical field $E(t)$ [10]. The two remaining parameters in the LK-equations are $\eta = \tau_p\gamma$ and $T = \tau_s/\tau_p$. The power of the laser is $P(t) = |E(t)|^2$ and we denote the phase of the laser field by $\phi(t)$. In our scheme of two coupled lasers, the coupled LK equations can be written as

$$\frac{dE_1(t)}{dt} = (1+i\alpha)N_1E_1(t) + \eta_1 e^{-i\omega_1\tau_1}E_2(t-\tau_1),$$
$$T\frac{dN_1(t)}{dt} = J_1 - N_1(t) - [2N_1(t)+1]|E_1(t)|^2,$$
$$\frac{dE_2(t)}{dt} = (1+i\alpha)N_2E_2(t) + \eta_1 e^{-i\omega_1\tau_1}E_1(t-\tau_1) + \eta_2 e^{-i\omega_2\tau_2}E_2(t-\tau_2),$$
$$T\frac{dN_2(t)}{dt} = J_2 - N_2(t) - [2N_2(t)+1]|E_2(t)|^2, \qquad (2)$$

where $\tau_1 = l_1/c$ and $\tau_2 = 2l_2/c$. In our numerical experiments we set the parameters such that the individual lasers are near their thresholds: $T = 1000$, $\alpha = 6$, and $J_1, J_2 < 0.01$. The bifurcation parameters are $\eta_{1,2}$ and $\tau_{1,2}$. We utilize the forth-order Adams–Bashford–Moulton (ABM) predictor–corrector method [11,12] with step size $dt = \tau_1/n_p$ to integrate Eq. (2), where

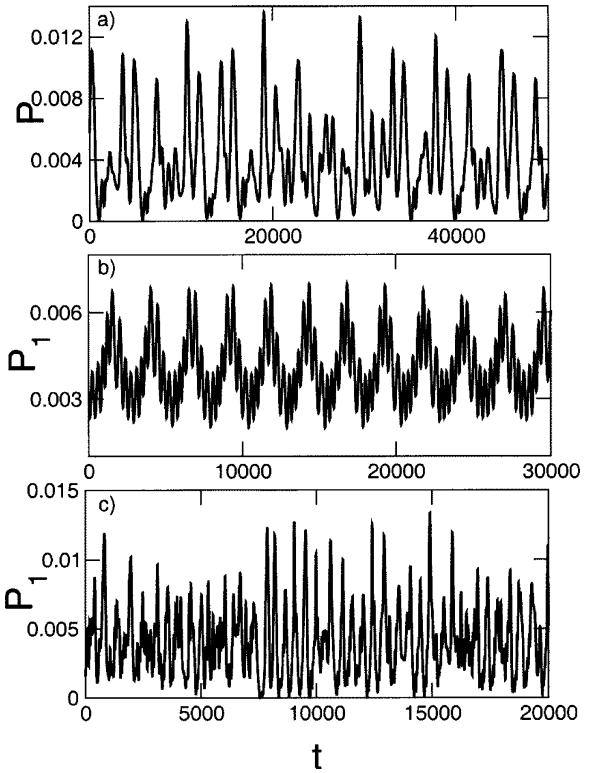

Fig. 2. Time traces of the power output: (a) uncoupled laser, (b) coupled system (Eq. (2)) in a locked regime (see Fig. 3) where the amplitude of the laser field has been modulated in a desirable manner so that the power output no longer drops down to zero, and (c) coupled system in an unlocked regime. Time is in units of the photon lifetime τ_p (see [8]).

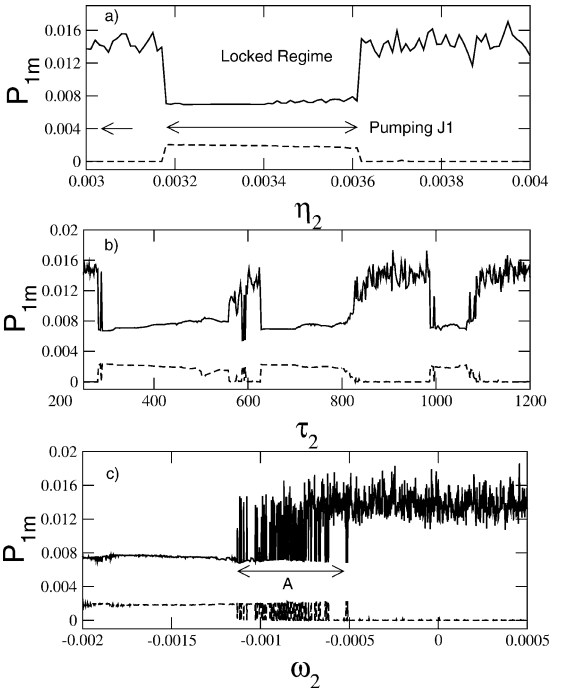

Fig. 3. For the coupled laser system, the maximum (solid line) and minimum (dotted line) values of the power output versus (a) η_2 for fixed $\tau_2 = 1000$, (b) τ_2 for fixed $\eta_2 = 3.3 \times 10^{-3}$, and (c) ω_2 for $\omega_1\tau_1 = -1$, $\tau_1 = \tau_2 = 1000$. The locked regimes are those where the power dropouts associated with LFFs are avoided. Note that in (c), there are substantial amounts of frequency detuning between the two lasers. The wild fluctuations in power output in region A (not a locked region) suggests the existence of two LFF attractors with complicated basins.

$n_p = 1000$ is chosen to be the number of initial conditions in the time intervals $-\tau_{1,2} \leqslant t < 0$. In what follows, we use symbols P, N and Z without subscript as for uncoupled lasers while symbols with subscripts for coupled lasers.

We now demonstrate that the coupling scheme illustrated in Fig. 1 can modulate the laser field in a desirable manner so that the output power no longer drops down to zero. To compare the performance of the coupled laser system with that of an individual laser with optical feedback, we refer to a laser described by the original LK-equations with feedback parameter η, τ, and J as *uncoupled*, while these by Eq. (2) as *coupled*. Fig. 2(a) shows for an uncoupled laser with $\eta = 2 \times 10^{-3}$, $\tau = 1000$, and $J = 4 \times 10^{-3}$, a typical time trace of the laser output power $P(t)$, where we see that power dropouts occur at random times. In contrast, the output power $P_1(t)$ of the coupled laser system can be made more regular and its minimum values are bounded away from zero, as shown in Fig. 2(b), where parameters values are set to be: $\tau_1 = \tau_2 = 1000$, $J_1 = 4 \times 10^{-3}$, $J_2 = 2 \times 10^{-3}$, $\eta_1 = 2 \times 10^{-3}$, and $\eta_2 = 3.3 \times 10^{-3}$. Thus, although LFFs are still present in the coupled system, they are modulated in a desirable way. Comparison between Fig. 2(a) and (b) indicates that, while the amplitude of the power fluctuations is reduced in the coupled system, its average power output remains approximately the same as that of the uncoupled laser. Thus, the coupled laser system can operate without degrading in power output but with the desirable feature that the instantaneous power will never be zero. The features in Fig. 2(b) in fact occur in finite parameter regions, as shown in Fig. 3(a), (b), and (c), where the maxi-

mum and minimum values of the power output of the coupled laser system are plotted versus the feedback strength η_2, the delay time τ_2, and the frequency ω_2, respectively. We see that there are various *locked* parameter regions of finite size in which amplitude modulation occurs. A feature is that if we wish to have an average output at some specific level, we can fix J_1 at that level and then vary other parameters of L_2 so that the system is in a locked regime. In the unlocked regime the power fluctuations are irregular and they drop near to zero as shown in Fig. 2(c). Varying other parameters, such as J_1, τ_1 and α, results in a similar behavior. We have also found that in the locked regime the two lasers exhibit the following behavior: a small distance between two nearby phase-space points for one laser tends to correspond to a small distance in another laser. This is in fact a generalized synchronous behavior [13].

We now give a heuristic theory, based on dynamics, for the numerically observed modulation of laser oscillations. For an uncoupled laser, the set of stationary solutions constitutes the most fundamental dynamical invariant sets responsible for LFFs [12,14], which are determined by the following set of transcendental equations:

$$\begin{aligned} N_s &= -\eta\cos(\phi_0 + Z_s),\\ N_s &= (J - P_s)/(1 + 2P_s),\\ Z_s &= -\eta\tau\sqrt{1+\alpha^2}\sin\bigl[Z_s + \phi_0 + \tan^{-1}\alpha\bigr],\\ \eta^2 &= N_s^2 + (Z_s/\tau - \alpha N_s)^2, \end{aligned} \tag{3}$$

where the phase-delay variable is $Z(t) \equiv \phi(t) - \phi(t-\tau)$ and $Z_s = (\omega_s - \omega_0)\tau$. The fixed points are typically distributed along an elliptic curve in the (Z, N) plane. The physical nature of these fixed points changes with a bifurcation parameter, say η. The following is a typical scenario [15]. As η is increased from zero, a saddle-node bifurcation occurs, where a pair of fixed points, one stable and another unstable, is created. The stable one is a maximum gain mode (MGM) while the unstable fixed point is an antimode. As η is increased further, the antimode remains so but the stable fixed point can become an unstable one via a Hopf bifurcation, usually called an external-cavity mode (ECM). For a given parameter value, typically there are an MGM, a number of ECMs and antimodes. The dynamical interplay among these distinct fixed points, which is determined by their eigenvalues, gives rise to phenomenon such as LFFs [14,15].

A trajectory in the phase space can visit the neighborhoods of ECMs and antimodes but can never stay there for a long time because these fixed points are unstable. Typically, there are multiple coexisting attractors, such as those giving rise to LFFs (the LFF attractors) and the MGM attractor [12,15]. The basin of the MGM attractor is, however, small in the phase space, which means that it is difficult to physically place the initial state of the laser near the MGM attractor. LFFs arise when the trajectory wanders on an LFF attractor whose basin is not dynamically connected with the basin of the MGM attractor, as shown in Fig. 4(a) and (b) for the uncoupled lasers L_1 and L_2 at the parameters $\eta = 2\times10^{-3}$, $J = 4\times10^{-3}$ and $\eta = 3.3\times10^{-3}$, $J = 2\times10^{-3}$, respectively. The plots in Fig. 4(a) and (b) represent the LFF attractors [14,15]. When these two lasers are coupled together with a time delay, the ranges in the Z–N plane of these attractors are reduced dramatically, as shown in Fig. 4(c), where the upper-right attractor corresponds to the dynamics of laser L_1 in (Z_1, N_1)-plane and the lower-left attractor to that of L_2 in the (Z_2, N_2)-plane. We observe that, due to coupling, both lasers operate more locally in the phase space: laser L_2 tends to stay near the MGM, while the dynamical trajectories of L_1 (its output power is the one for the whole coupled system) are confined in a phase-space region where the corresponding power can never be zero. Examination using a Poincaré surface of section indicates that these small attractors are quasiperiodic, as shown in Fig. 4(d) for laser L_1. This is then analogous to the phenomenon of amplitude death [4,5] with the distinction that, in such a case, the dynamical invariant set changes from a limit cycle to a steady state, whereas in our case, an LFF attractor, which is typically chaotic [15], is converted into a quasiperiodic one via time-delayed coupling. Fig. 5 shows a bifurcation diagram, where the set of local maxima of $P_1(t)$ is plotted versus the coupling parameter η_2. For $\eta_2 < \eta_{2c}$, $P_1(t)$ is apparently chaotic, while for $\eta_2 > \eta_{2c}$, $P_1(t)$ is regular (quasiperiodic). The origin of quasiperiodic motion may be related to the existence of "backbone" regular dynamics associated with LFFs when the pumping current is close to the solitary threshold of the laser [16].

The wild fluctuations in the power output of the coupled laser system in region A in Fig. 3(c) indicates

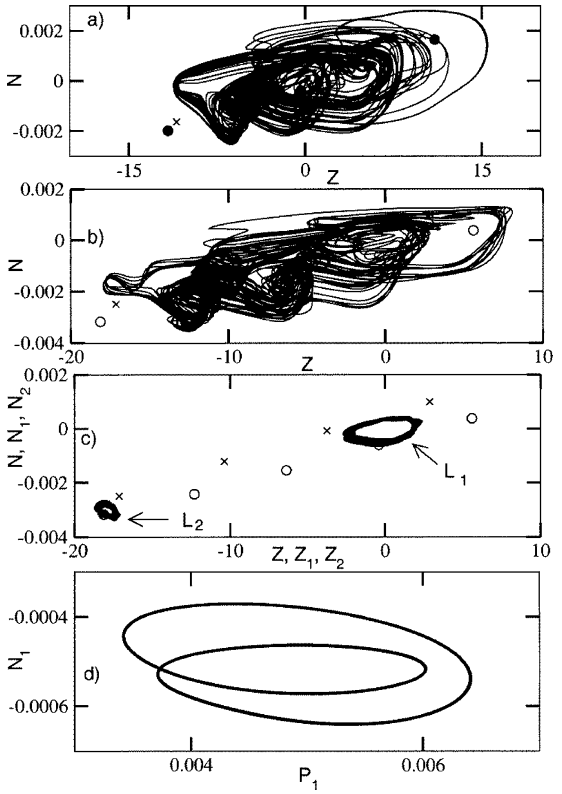

Fig. 4. LFF attractors projected in the Z–N plane: (a) laser L_1, absence of L_2, with parameters $\eta = 2 \times 10^{-3}$ and $J = 4 \times 10^{-3}$; (b) laser L_2, in absence of L_1, with parameters $\eta = 3.3 \times 10^{-3}$ and $J = 2 \times 10^{-3}$. (c) The trajectories of L_1 and L_2 in plane Z_1–N_1 and Z_2–N_2 plane, respectively, of coupled systems at $\omega_2 = -1.5 \times 10^{-3}$. The fixed points in Z–N plane are those of the uncoupled laser L_2 of (b). (d) The Poincaré section of the trajectory in (c) at $Z_1 = 0$, indicating its quasiperiodic nature.

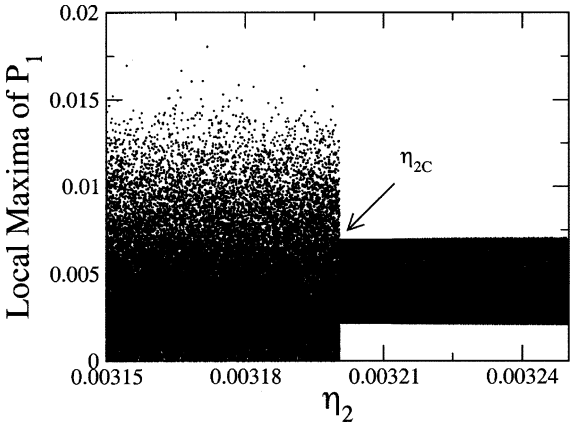

Fig. 5. A typical bifurcation diagram for amplitude modulation: local maxima of $P_1(t)$ versus the coupling parameter η_2. For $\eta_2 < \eta_{2c}$, $P_1(t)$ is apparently chaotic, while for $\eta_2 > \eta_{2c}$, $P_1(t)$ is regular (quasiperiodic). Other parameters are the same as for Fig. 3(a).

the presence of two coexisting attractors: one similar to that in a locked regime (Fig. 2(b)) and another in an unlocked regime (Fig. 2(c)). A small change in the parameter ω_2 can lead to a completely different attractor with distinct power output, implying complicated basins of these attractors [17].

Physically, the disappearance of complete power dropouts in our coupled laser system can be understood by noticing that a semiconductor laser, when not subject to any optical feedback, can generally maintain stable power output. LFFs occur when there is optical feedback. When two lasers are coupled as in our scheme (Fig. 1), if the interaction of the optical fields is such that, on average, the feedback into laser L_1 reaches approximately zero, then this laser essentially behaves dynamically like one without any feedback, generating stable output with no power dropouts. For laser L_1, laser L_2 provides a physical means for generating close-to-zero feedback through the *dynamical coupling* between the lasers.

The above physical picture provides a heuristic approach to understand the bifurcation responsible for the amplitude-modulation phenomenon. As the coupling parameter η_2 changes so that amplitude modulation occurs, effectively the amount of feedback into the output laser is decreased. To make the analysis feasible, we consider a simplified version of the LK equations [18]. In particular, we write the complex electrical field as: $E(t) = R(t)\exp[i\phi(t)]$, where $R(t)$ and $\phi(t)$ are the field amplitude and phase, respectively. Since typically, the time variation of the phase is much faster than that of the amplitude, the following approximation can be used [18]: $R(t-\tau) \sim R(t)$, and $\dot{\phi} \sim z(t)/\tau + \dot{z}(t)/2$, where $z(t) = \phi(t) - \phi(t-\tau)$ is the phase delay. By choosing the laser power $P(t) = R^2(t)$, the carrier density $n(t)$, and the phase delay $z(t)$ as the new set of dynamical variables, one can then arrive at the following three-dimensional model [18]:

$$\frac{dP(t)}{dt} = 2\big[n(t) + \eta\cos\big(z(t) + \phi_0\big)\big]P(t),$$

$$\frac{Tdn(t)}{dt} = J - n(t) - \big(2n(t) + 1\big)P(t),$$

$$\frac{dz(t)}{dt} = 2\left[-\frac{z(t)}{\tau} + \alpha n(t) - \eta \sin\bigl(z(t) + \phi_0\bigr)\right], \quad (4)$$

which possesses the same steady state solutions as those in the full LK equations, as determined by Eq. (3).

The steady state solutions are the key to understanding the bifurcation leading to amplitude modulation. Eq. (3) is a set of transcendental equations which gives a series of solutions denoted by (P_s, n_s, z_s), where a physical solution satisfies the condition $n_s \leqslant J$. The stabilities of the fixed points are determined by the eigenvalues $\bar{\lambda}$ that are solutions of

$$\bar{\lambda}^3 + A\bar{\lambda}^2 + B\bar{\lambda} + C = 0,$$

where A, B, and C are given by:

$$A = \frac{1}{\tau} + \eta\cos(z_s + \phi_0) + \frac{1 + 2P_s}{2T},$$
$$B = \frac{1 + 2P_s}{2T}\left[\frac{1}{\tau} + \eta\cos(z_s + \phi_0)\right] + P_s\frac{1 + 2n_s}{2T},$$
$$C = P_s\frac{1 + 2n_s}{2T} \times \left[\frac{1}{\tau} + \eta\cos(z_s + \phi_0) - \eta\alpha\sin(z_s + \phi_0)\right]. \quad (5)$$

There are only two possibilities for the three eigenvalues of a fixed point: either all three are real or, one is real, say $\bar{\lambda}_1 = \lambda$, and the other two are complex, say $\bar{\lambda}_{2,3} = r \pm is$, where r and s are the real and imaginary parts, respectively.

We choose the feedback parameter η as the bifurcation parameter and describe how these fixed points are created as the bifurcation parameter η is increased from zero. For illustrative purpose we set the other parameters as $\tau = 1000$, $T = 1000$, $\alpha = 6.0$, $J = 0.001$, and $\phi_0 = \omega_0\tau = -1$. The solutions of Eq. (3) can be represented graphically as the intersecting points between the solid curve (the third equation) and the dotted line, as shown in Fig. 6(a), where the number of solutions is proportional to $\eta\tau\sqrt{\alpha^2 + 1}$. Of particular importance is the parameter interval in between two successive tangencies of the dotted straight line with two adjacent branches of the sine curve. For instance, Fig. 6(a) corresponds to an η value in between the tangencies of the dotted line with the two leftmost branches of the sine curve. Here we analyze one such parameter interval. The mathematical condition for a tangency to occur is: $\lambda = 0$ and $C = 0$, which in fact

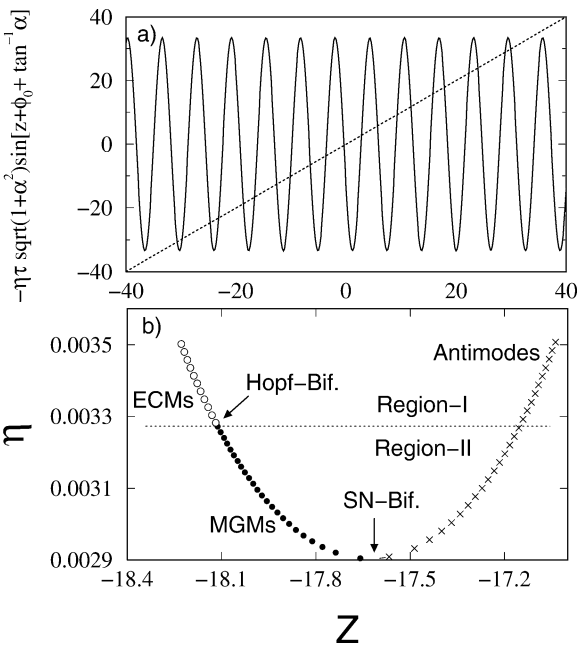

Fig. 6. For $\eta = 0.0055$: (a) a graphical representation of the transcendental equation (3) (the third equation); (b) the MGMs (•) and ECMs (○), and the antimodes (×). The horizontal dotted line divides the parameter space into two regions: in Region I the LFFs are sustained, while in Region II the LFFs are transient.

leads to a saddle-node bifurcation where a pair of fixed points, one stable and another unstable, is created. The stable one is an MGM while the unstable fixed point is an antimode. As η is increased further from the saddle-node bifurcation point, the antimode remains so but the stable fixed point can be an MGM for only a small range of values of η. The evolution of a typical saddle-node pair is shown in Fig. 6(b) in the η–z plane, where for this particular pair a Hopf bifurcation occurs at $\eta \approx 0.00328$ (the horizontal dotted line) which turns the original stable fixed point (MGM) into an unstable one (in fact an ECM). At the Hopf bifurcation, the coefficients A, B, and C in Eq. (5) satisfy: $A > 0$, $C > 0$, and $C - AB = 0$, where $\omega^2 = C$ and ω is the frequency of the limit cycle at the bifurcation point, and the value of r becomes positive from the negative side. The Hopf bifurcation naturally divides the parameter interval into two distinct regions: Region I (from the Hopf bifurcation to next saddle-node bifurcation, above the dotted line) and Region II (from the original saddle-node bifurcation to the Hopf bifurcation, below the dotted line). At the top end of

Region I, a new saddle-node bifurcation occurs, after which the situation depicted in Fig. 6(b) repeats for the newly created saddle-node pair. The antimodes and ECMs, after being created, remain in the phase space for a much larger parameter interval than those for the MGMs. The LFF attractors in Region I are typically chaotic while those in Region II are regular [15]. *Thus we see that the amplitude modulation phenomenon for which a chaotic LFF attractor is converted into a regular one, is triggered by a Hopf bifurcation.*

In summary, we have presented evidence for amplitude modulation in a pair of optically coupled, external-cavity semiconductor lasers. The phenomenon occurs in parameter regimes of positive measure. The scheme is in fact suitable for experimental test. The two lasers and the mirror can be placed at fixed distances so that the whole system falls in a locking regime. Such a laser system possesses all advantages associated with optical feedback, but with no power dropouts. While we assume identical lasers in our scheme, we find that the condition of identity can be relaxed to certain extent. For instance, effective elimination of power dropouts can be achieved even when the mismatch between the two lasers is as large as 10% (say, we set $\alpha_1 = 6$ and $\alpha_2 = 6.5$). However, in the presence of larger mismatches, the ranges of the locked regimes are too small for the scheme to be practically useful.

Finally, we stress the difference between our work and the existing works on amplitude-death [4,5]. Despite the common coupling scheme employing time-delayed signals, all existing works are for limit-cycle oscillators, while ours deals with *chaotic* oscillators. Previous studies indicate that LFFs in external-cavity semiconductor lasers are the result of various chaotic transitions [12,14]: the dynamics of such lasers in the LFF regime are thus typically chaotic. As we have demonstrated, time-delayed coupling can convert the chaotic oscillation of the laser field with power dropouts into quasiperiodic motion without power dropouts. We have thus uncovered a more general type of amplitude-modulation phenomenon in time-delayed coupled nonlinear oscillators: transition from chaotic oscillations to quasiperiodic motions. We think this is a nontrivial generalization of the conventional amplitude-death phenomenon that occurs in limit-cycle oscillators.

Acknowledgement

A.P. and Y.C.L. were supported by AFOSR under Grant No. F49620-98-1-0400.

References

[1] K. Bar-Eli, Physica D 14 (1985) 242.
[2] R.E. Mirollo, S.H. Strogatz, J. Stat. Phys. 60 (1990) 245.
[3] G.B. Ermentrout, Physica D 41 (1990) 219;
D.G. Aronson, G.B. Ermentrout, N. Koppel, Physica D 41 (1990) 403.
[4] D.V. Ramana Reddy, A. Sen, G.L. Johnston, Phys. Rev. Lett. 80 (1998) 5109.
[5] R. Herrero, M. Figueras, J. Rius, F. Pi, G. Orriols, Phys. Rev. Lett. 84 (2000) 5312;
D.V. Ramana Reddy, A. Sen, G.L. Johnston, Phys. Rev. Lett. 85 (2000) 3381.
[6] K.R. Preston, K.C. Woolard, K.H. Kameron, Electron. Lett. 17 (1981) 931;
K. Kikuchi, T. Okoshi, Electron. Lett. 18 (1982) 10;
L. Goldberg, H.F. Tylor, A.A. Dandridge, J.F. Weller, R.O. Miles, IEEE J. Quantum Electron. 18 (1982) 555;
S. Saito, O. Nilsson, Y. Yamamoto, IEEE J. Quantum Electron. 18 (1982) 961;
R. Wyatt, W.J. Devlin, Electron Lett. 19 (1983) 110;
F. Favre, D. Le Guen, Elecron. Lett. 19 (1983) 663;
D. Lenstra, B.H. Verbeek, A.J. den Boef, IEEE J. Quantum Electron. 21 (1985) 674.
[7] R. Lang, K. Kobayashi, IEEE J. Quantum Electron. 16 (1980) 347.
[8] P.M. Alsing, V. Kovanis, A. Gavrielides, T. Erneux, Phys. Rev. A 53 (1996) 4429.
[9] C.H. Henery, IEEE J. Quantum Electron. 18 (1982) 259;
C. Masoller, IEEE J. Quantum Electron. 33 (1997) 796.
[10] B. Tromborg, J. Mørk, IEEE J. Quantum Electron. 33 (1990) 642.
[11] W.H. Beyer, CRC Standard Mathematical Tables and Formulae, 29th Edition, CRC Press, Boca Raton, FL, 1991.
[12] R.L. Davidchack, Y.-C. Lai, A. Gavrielides, V. Kovanis, Physica D 145 (2000) 130.
[13] N.F. Rulkov, M.M. Sushchik, L.S. Tsimring, H.D.I. Abarbanel, Phys. Rev. E 51 (1995) 980.
[14] T. Sano, Phys. Rev. A 50 (1994) 2719.
[15] A. Prasad, Y.-C. Lai, A. Gavrielides, V. Kovanis, J. Opt. B: Quantum Semiclass. Opt. 3 (2001) 242.
[16] R.L. Davidchack, Y.-C. Lai, A. Gavrielides, V. Kovanis, Phys. Rev. E 63 (2001) 056206.
[17] A. Prasad, Y.-C. Lai, A. Gavrielides, V. Kovanis, preprint (2002).
[18] G. Huyet, P. Porta, S.P. Hegart, J.G. McInerney, F. Holland, Opt. Commun. 180 (2000) 339.